Chapter 8
Grains and Grain Boundaries

8.1 Grains in solids 2
8.1.1 Fabrication of polycrystalline solids 2
Polycrystalline metals 2
Polycrystalline ceramics 3
8.1.2 Microscopic structure of grain boundaries 3
Small-angle grain boundary 4
Large-angle grain boundary 5
8.1.3 Simplified representation of a grain 6
Tetrakaidecahedra 7
Columnar grains 8
Elongated Grains 9
8.2 Grain size distribution and grain growth 9
8.2.1 Hillert's model 11
8.2.2 Grain-size distribution. 12
8.2.3 Average grain size 14
8.2.4 Grain Growth 15
8.3 Grain Boundary Mobility 15
8.4 Grain Boundary Diffusion 17
8.4.1 Measurement of the Grain-Boundary Diffusivity 17
8.4.2 Effect of Grain Boundary Diffusion on Fission Product Release 19
8.5 Sintering 24
References 27

8.1 Grains in solids

Nearly all inorganic materials (metals and ceramics; glasses excepted) consist of many tiny particles of the constituent solid tightly bonded together. The particles are small single crystals of dimensions generally between 5 and 100 μm randomly oriented in the solid. These particles are called *grains* and the solid that they make up is termed *polycrystalline*. By randomly oriented is meant a mismatch between the lattice vectors of adjacent grains. The interfaces between grains constitute the *grain boundaries* of the solid.

8.1.1 Fabrication of polycrystalline solids

Polycrystalline solids are mainly formed in one of two ways. Metals and alloys crystallize into the solid by cooling from the liquid phase (top diagrams of Fig. 8.1). Ceramics, on the other hand, are produced from pressed compacts of powders by heating at high temperature. The lower diagrams of Fig. 8.1 show the powder method. .

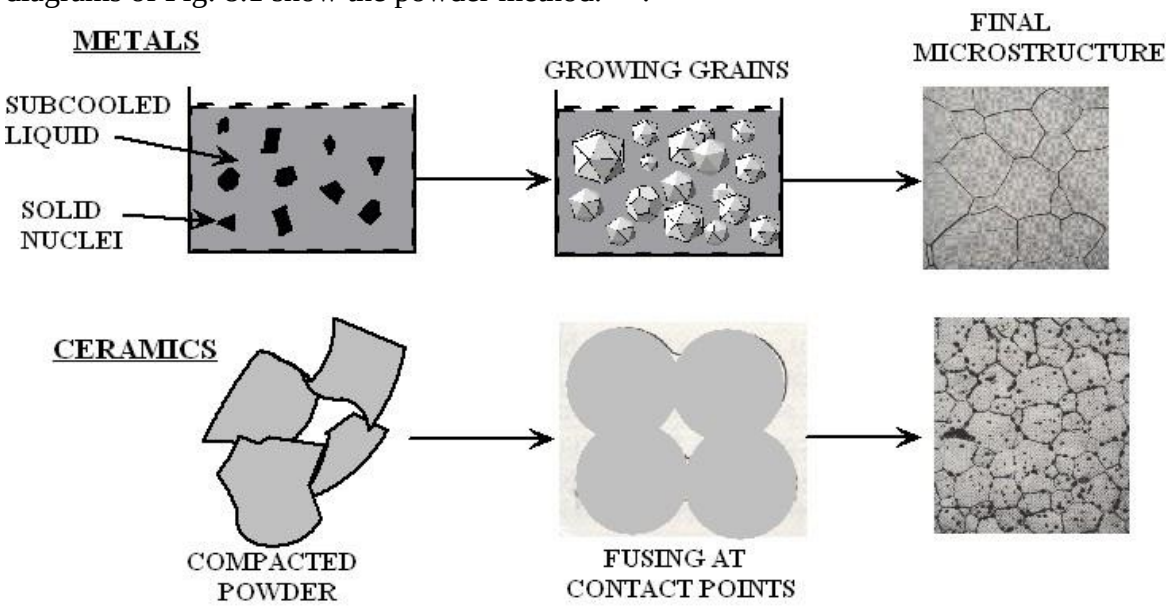

Fig. 8.1 Methods of producing high-density polycrystalline bodies of metals and ceramics

There are many other methods for producing surface layers, including electroplating, chemical vapor deposition, plasma spraying and sputter deposition. Here we restrict attention to the bulk methods shown in Fig. 8.1.

Polycrystalline metals

Producing metals begins with the metal (or alloy) in the molten state. When the metal is cooled below the melting point , the liquid becomes unstable thermodynamically with respect to the solid phase. Nuclei of the solid begin to form. After a sufficient concentration of nuclei have

been created, the nucleation process ceases and the existing nuclei begin to grow into small single crystals of the solid metal. Eventually these crystallites touch other with different crystallographic orientations. Upon complete solidification, the solid microstructure reflects the random union of adjacent grains, as shown in the upper right hand micrograph in Fig. 8.1. The pattern in the grains of the final microstructure of the metal is an artifact or polishing and etching in preparations for microscopy; the grains are featureless. However, the lines are real and reveal *grain boundaries*. The average size of the grains in the metal microstructure shown in Fig. 8.1 is 70 μm.
Although Fig 8.1 and the above description deal with homogeneous nucleation, heterogenous nucleation starting on the container walls is the primary method for fabricating metals.

Polycrystalline ceramics

The starting material and the mechanism of producing ceramic polycrystals are very different from those of metals. Whatever the original form, the ionic compound is ground to a fine powder and compacted in a press. At this stage, the porosity (or fraction of the theoretical density of the material) is low (~ 50%). Densification is accomplished by heating the compacted powder pellets in a furnace in a process called *sintering*. Initially, the pieces of powder fuse at their points of contact. This forms a region with a smaller radius of curvature than that of the free surfaces. Hence, the Gibbs energy of the former is greater than that of the latter. This thermodynamic driving force causes molecules of the solid to flow from the free surfaces to the fused points of contact, which results in growth of the fused zone. During this stage, some of the gas in the sintering atmosphere becomes trapped as more-or-less spherical cavities in the solid. This trapped gas is termed *closed porosity*. In addition, channels in the interior of the body lead to a free surface. This is *open porosity*. As sintering continues, the initial particles assume the structure of small single crystals. As this compaction takes place, the porosity of the body (and its volume) diminishes. The final microstructure of a typical sintered ceramic is shown in the lower right of Fig. 8.1. The small black dots are the residual closed porosity, which cannot be eliminated because the gas trapped in the pores exerts an outward pressure that just balances the inward force arising from surface tension of the curved inner surface. Thus, obtaining 100% dense ceramic bodies is generally not possible.

Powder-metallurgy is also a specialized method for fabricating oxide-dispersion ferritic alloys, which are possible cladding metals for advanced fuel for light-water reactors

8.1.2 Microscopic structure of grain boundaries

The atomic structure of a grain boundary is of one of two types: a *small-angle* structure or a *large-angle* structure. Grain boundaries can also be classified according to the type of dislocation of which they appear to be constructed. *Tilt* boundaries can be considered to be vertical accumulations of edge dislocations whilst *twist* boundaries are arrays of screw dislocations. However, the boundaries are not actually made this way (see above). Steps and ledges affect the curvature of the grain boundary.

Small-angle grain boundary

A schematic representation of a small-angle grain boundary is shown in Fig. 8.2
The boundary is equivalent to a "wall" formed by stacking parallel edge dislocations of the same sign (upside-down tees) in a vertical array. The grain on the left is tilted with respect to the one on the right by an angle θ. The spacing between dislocations, λ_d, is related to the Burger's vector (b) and the angle between the two grains (θ) on the right of Fig. 8.2. The relation is:

$$\lambda_d = \frac{b}{2\sin(\theta/2)} \cong \frac{b}{\theta} \tag{8.1}$$

The dislocation wall model of a grain boundary fails when the angle θ is greater than ~ 15°. For this misorientation angle and b ~ 0.3 nm, the vertical spacing of the edge dislocations is ~ 1.1 nm. This is approximately four lattice constants.

The energy per unit area of the small-angle grain boundary depends on the dislocation spacing. The total energy per unit length of a screw dislocation is given in Sect 7.6 of Chap. 7. To apply this formula to the energy per unit area of the vertical array of dislocations, one need only divide by the spacing λ_d (because there are $1/\lambda_d$ dislocations per unit height). With a slight modification for application to edge dislocations, and with the extent of the elastic strain energy field restricted to the separation distance λ_d, the energy per unit area of the boundary is:

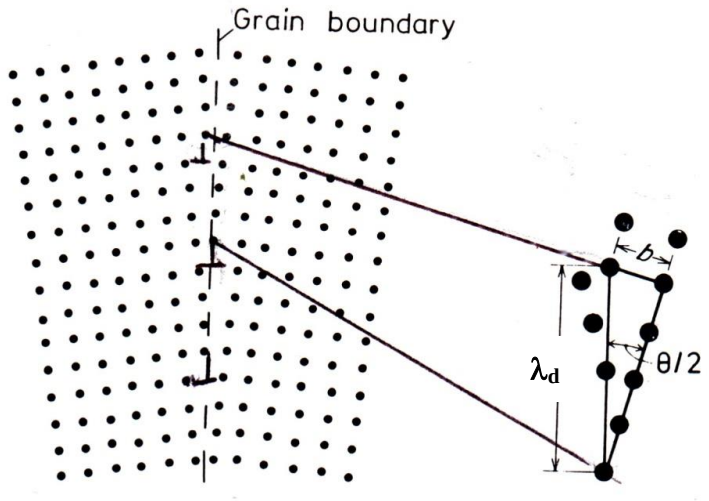

Fig 8.2 A small-angle grain boundary in a cubic crystal (Ref. 1)

$$\gamma_{gb} = \frac{E_d}{\lambda_d} = \frac{1}{\lambda_d}\left[E_{core} + Gb^2\frac{\ln(\lambda_d/b)}{4\pi(1-\nu)}\right] = \frac{\theta E_{core}}{b} - \frac{G b \theta \ln\theta}{4\pi(1-\nu)} \tag{8.2}$$

E_{core} is the core energy contained within a radial distance from the centerline of the dislocation approximately equal to the Burger's vector. The core energy cannot be described by elasticity

theory, but is about 15% of the second term. In the elastic strain energy term, G is the shear modulus and ν is Poisson's ratio.

Example #1 – grain-boundary energy - calculate the grain boundary energy for b = 0.3 nm, $G = 8x10^{10}$ Pa. and two angles, $\theta = 5^o$ and 10^o
Using these values in Eq (8.2), the elastic term on the right hand side is 0.6 J/m^2 for $\theta = 5^o$ and 0.84 J/m^2 for $\theta = 10^o$. Assuming that the core energy adds 15% to this value, the energy per unit area is 0.7 or 1.0 J/m^2. The accepted value for UO_2 is $\gamma_{gb} \sim 0.3$ /m$^{2.}$

Large-angle grain boundary

When the growing grains meet at a mismatch angle greater than ~15^o, the dislocation wall model of the small-angle grain boundary is no longer applicable. Instead, extensive computer calculations of the type called *molecular statics* (Chap. 14) are needed. In this method, atoms in or near a grain boundary are permitted to interact pairwise with a known interatomic potential. Two grains are joined at a specified misorientation angle and the energy of the grain boundary is determined by summing the interaction energies of each atom with all others. This summation is carried over atoms in the grain boundary, i.e., those whose positions are not part of the adjacent perfect crystal structure. The atoms are allowed to move, or to "relax" until the configuration with the lowest energy is achieved. Figure 8.3 shows the computed relaxed structures of large-angle (37^o misorientation angle) grain boundaries in NiO (left) and in Ag (right).

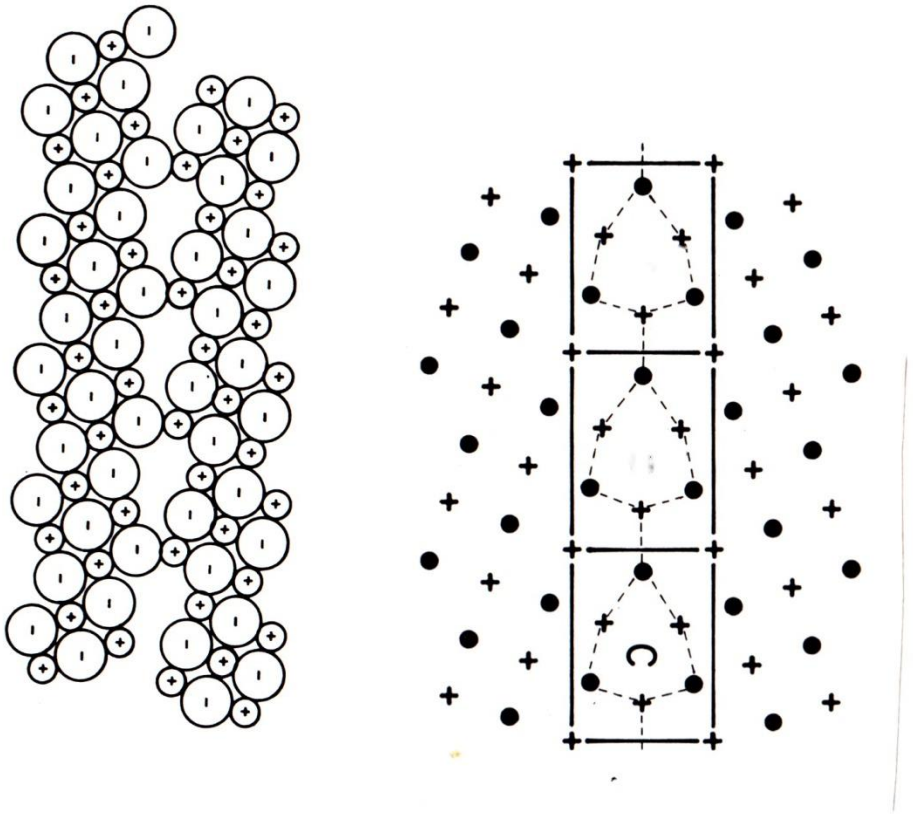

(a) ceramic (NiO) **(b) metal (Ag)**

Fig. 8.3 Structure of large-angle grain boundary (Ref. 1)

The boxes in the metal grain boundary delineate the repeating structure, which, in 3D is a trigonal prism. The dots and crosses represent different atom layers.
(The atomic planes of the lattice are misaligned only in the plane of the paper).

The sizes of the circles representing the anions and cations are proportional to their ionic radii. The anion (oxygen) has a large ionic radius because it is doubly negatively charged. The positively-charged cation (Ni) is much smaller. The grain boundaries in Fig. 8.3 are called *tilt* boundaries.

.A second type of misalignment is produced by rotating one of the adjacent grains in a plane perpendicular to the paper. This produces a *twist* boundary. A twist boundary in an elemental crystal is shown in Fig.8.4.

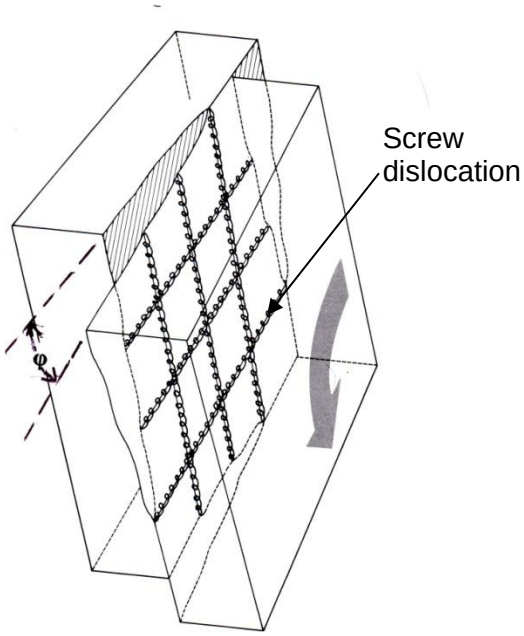

Fig. 8.4 Twist boundary with misorientation angle φ (Ref. 2)

The pure twist grain boundary is formed by interlaced screw dislocations in the plane of the boundary, much as the tilt boundary of Fig. 8.2 consists of stacked edge dislocations in the boundary plane.

No computer simulations of even a simple twist boundary have been performed, probably because of the complexity of the atom arrangements. Real grain boundaries are even more complex because they generally have both tilt and twist components. To describe such grain boundaries, both the tilt angle θ and the twist angle φ need to be specified. Current belief is that grain boundaries are made up of distinct atomic arrangements; they are not liquid-like disorganized regions as was previously thought.
Because of the mismatch of the crystal structures, the distance between adjacent grain faces in polycrystalline solids is greater than atom spacing inside the grain. This enlargement permits more rapid diffusion of defects and impurity atoms in the boundary than in the interior.

8.1.3 Simplified representation of a grain

Despite the irregularity of the grain boundaries, mathematical analyses of the effect of the grain structure on various properties of the solid often require simulating the grain as regular polyhedra. The choice of polyhedron is limited by two facts: i) in aggregates, it must be space-filling; ii) when cut along a plane surface, three boundaries must join at a point, as in the microstructure shown in Fig. 8.1. Rectangular parallelepipeds assembled as a brick wall does not even remotely resemble the 2-D structure of the grain boundaries.

Tetrakaidecahedra

A much closer fit is provided by the 14-sided polyhedron called a *tetrakaidecahedron*. This solid (Fig. 8.5**)** is an octahedron with equilateral triangles as faces and six corners cut off so that all 36 edges are of the same length *l*.

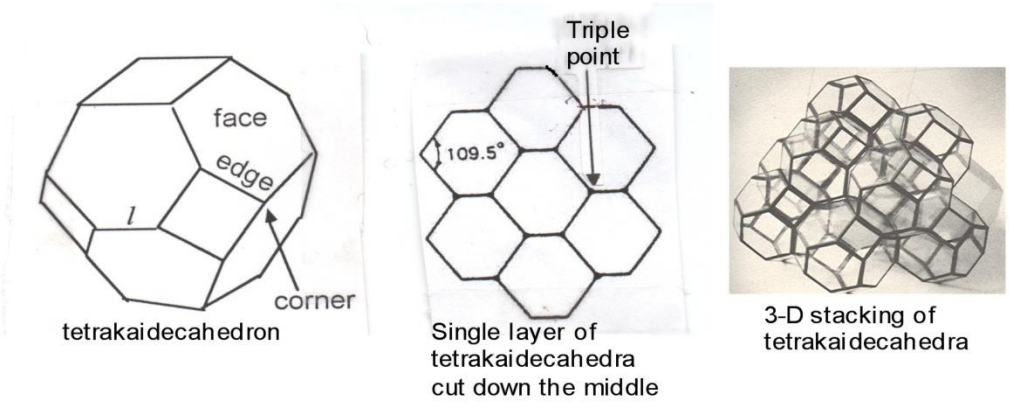

8.5 Representation of a grains as tetrakaidecahedra

The faces are made up of 6 squares and 8 regular hexagons. A layer of tetrakaidecahedra can be constructed by stacking the individual units hexagon-to-hexagon and square-to-square. When such a layer is sliced down the middle, the boundaries appear as seen in the middle drawing of Fig. 8.5. This reasonably resembles the structure shown in the micrographs on the right in Fig. 8.1. In particular, three boundaries join in a *triple point*[1]. The right hand drawing shows tetrakaidecahedra assembled in a 3-D structure, which is seen to be space-filling. The properties of the tetrakaidecahedron are:

$$\text{Volume} = 11.3\, l^3; \qquad \text{Surface area} = 26.8\, l^2$$

Nearly all theoretical models of processes in polycrystalline solids assume the grains to be spherical in shape. A close-packed assembly of spheres (i.e., the fcc or hcp lattices) occupies only 76% of the available space, and so is not a legitimate model of a polycrystal. However, the tetrakaidecahedron is a reasonably good approximation of a sphere, at least for the purpose of, say, a diffusion calculation. The radius of the spherical grain of the same volume as the tetrahedron is

$$R_{gr} = \left(\frac{11.3}{4\pi/3}\right)^{1/3} l \qquad \text{or} \qquad R_{gr} = 1.39l.$$

[1] the triple point is not the same as the *corner* identified in the left hand drawing of Fig. 8.5

A quantity often required in analysis of processes involving grains is the grain boundary area per unit volume of solid. If the grains were separated, this is simply the ratio of the surface area to the volume of the grain. However, when the grains are agglomerated in a polycrystalline solid, each grain boundary is shared between two adjacent grains, so:

Grain boundary area per unit volume of solid = $\frac{1}{2} \frac{26.8}{11.3} \times \frac{1.39}{R_{gr}} = \frac{1.65}{R_{gr}}$ (8.3) So far, the only grain shapes described had no preferential macroscopic or microscopic orientation in space; such grains are called *equiaxed*. However, certain types of processes that the polycrystalline solid is subjected to can alter one or both of these features.

Columnar grains

As the name implies, columnar grains are shaped like columns. They are formed by chemical or physical processes that occur in one direction. The base of the oxide scale formed by oxidation of zirconium, for example, consists of elongated grains preferentially oriented perpendicular to the metal surface. The best-known example of columnar grain formation in nuclear technology is the structure formed in nuclear fuels operated at very high power (as in fast breeder reactors). The steep temperature gradient in such fuels causes porosity to migrate up the temperature gradient by a vapor transport mechanism (material vaporizes from the hot side of the pore, diffuses through the intervening gas, and condenses on the cold side, thereby causing the pore to move up the temperature gradient). The left hand side of Fig. 8.6 shows flattened pores migrating from bottom to top, each leaving behind a columnar grain in its wake. The right hand side of this figure shows a low-magnification view of the columnar grain structure in an irradiated fuel pellet previously subjected to a steep temperature gradient (as large as 10^4 ^{o}C/cm).

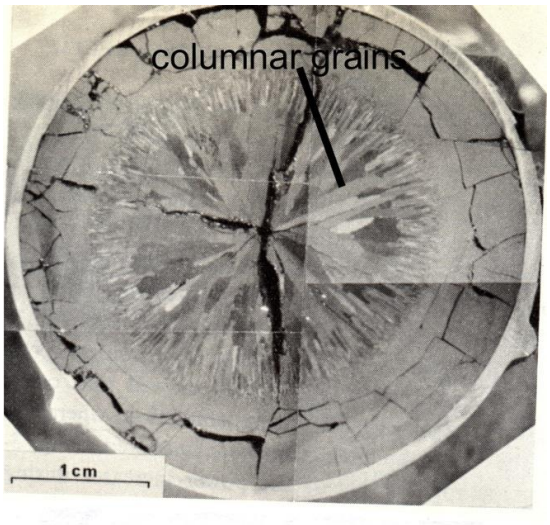

Fig. 8.6 Left: Migrating lenticular pores trailing columnar grains; Right: columnar grain structure following pore migration to the center of the fuel pellet

Elongated Grains

The microstructure of an elongated-grain structure is shown in Fig. 8.7 . The grains are clearly longer in the horizontal direction than in the vertical direction.

Fig. 8.7 Optical photomicrograph of iron exhibiting elongated grain structure - magnification 100X

Misshapen grains can be formed in a number of ways. The left hand panel of Fig. 8.8 illustrates how a compressive stress causes macroscopic deformation with accompanying elongation of the grains (lower left). The right hand panel shows the process on a microscopic scale.

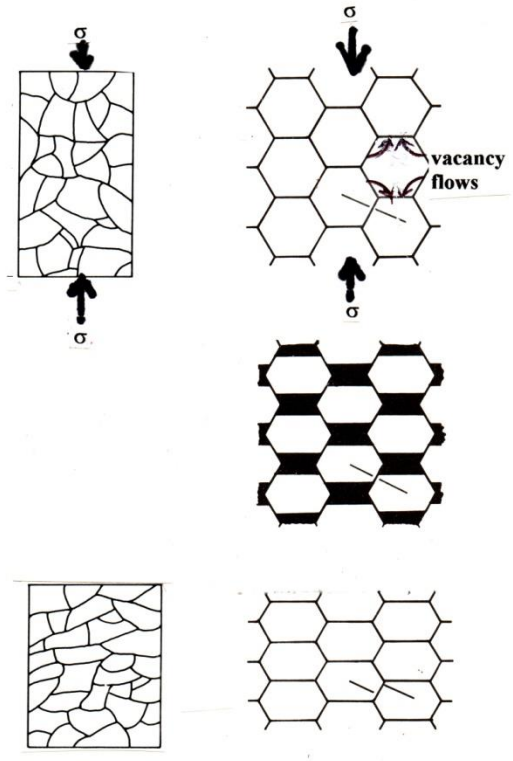

Fig. 8.8 Elongation of grains by creep due to a compressive stress

The compressive stress (σ) acts on the horizontal grain boundaries. On the slanted sides, the perpendicular stress component is ½ σ. Consequently, the vacancy concentration in the lattice immediately adjacent to the grain boundaries perpendicular to the stress is reduced from the stress-free value by a factor $\exp(-\sigma\Omega/R_gT)$ (Eq (4.9)) The reduction of the vacancy concentration adjacent to the grain boundaries that are slanted with respect to the stress axis is reduced by a factor $\exp(-\sigma\Omega/2R_gT)$. As a result, vacancies diffuse in the directions indicated on the upper right-hand drawing.

R.Olander and Arthur T. Motta

The atom flux countercurrent to the vacancy flux removes material from the solid adjacent to the horizontal grain boundary and the grains shrink in the vertical direction and grow in the horizontally. If vacancy diffusion were the only process active, voids at the horizontal grain boundaries would form, as indicated by the black zones in the middle drawing on the right hand side of Fig. 8.8. The compressive stress removes the voids and creates the elongated grains shown in the lower right hand drawing. This process is termed *Nabarro-Herring creep*. When the vacancy flows through the grain boundaries instead of through the grain, the process is referred to as *Coble creep.*

The diffusional creep process illustrated in Fig. 8.8 is slow, and is usually applied to ceramic bodies at high temperature (Sect. 11.4.4). For metals, a common procedure for rapidly changing the dimensions is the cold-forming process illustrated in Fig. 8.9. On the left of the rollers, the grains are equiaxed. After passage through the rollers, the grains are plastically deformed (by dislocation motion) into elongated shapes.

Another phenomenon that can occur during forming metal shapes is a realignment of the crystallographic orientation of the grains. In an anisotropic crystal such as the hexagonal close-packed structure (Fig. 2.3), deformation during fabrication can realign the directions of the crystal axes of the grains. In hcp zirconium, for example, the **c** direction is altered from random to unidirectional. This process is illustrated by the orientation of the arrowheads in Fig. 8.9, which represent the direction of a particular crystallographic direction. Upstream of the rollers, the directions of the crystal axes are random; downstream of the rollers, they point predominantly in the horizontal direction. The metal is said to have acquired *preferred orientation*. As a consequence, properties such as the yield strength and the coefficient of thermal expansion are different in the rolling direction from the other two directions.

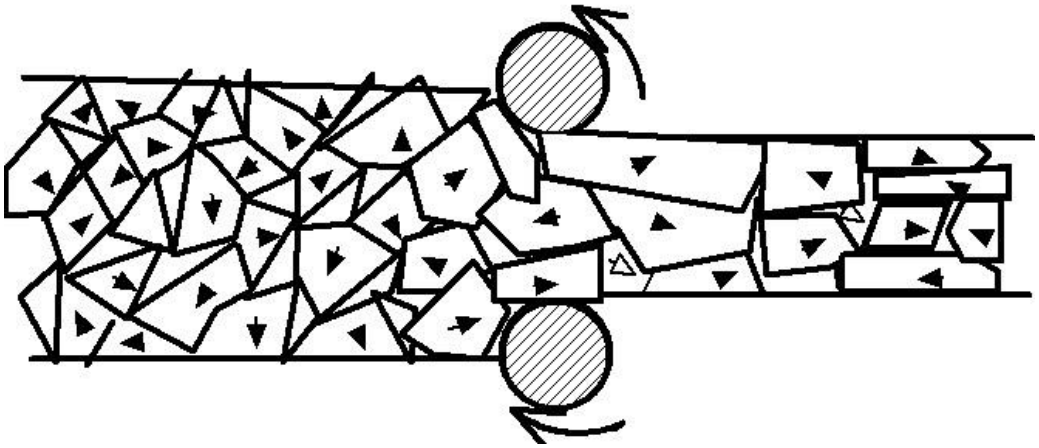

Fig. 8.9 Cold-working a plate

8.2 Grain size distribution and grain growth

It is evident from the photomicrographs in Fig. 8.1 that not all grains are the same size. Two features are important: the distribution of grain sizes and the average grain size. The latter is used

in all models of fuel behavior involving grains, and is deduced from the distribution of sizes. We follow the work of Hillert (3) for the size distribution, and later for the phenomenon of grain growth.

The first property needed for determining the size distribution is the behaviior of the grain boundaries . These move in a manner that reduces the area that the boundaries occupy in the solid. This spontaneous movement i reduces the Gibbs energy. The grain boundaries are regions of atomic mismatch and thus have a greater Gibbs energy than the perfect lattice. In the growth process, the small grains in the photomicrographs of Fig. 8.1 eventually disappear and the larger grains enlarge. In principle, this process continues until a perfect single crystal is obtained. In practice, the velocity of the grain boundaries becomes progressively smaller because they accumulate the "debris" in the solid such as pores, second phase precipitates and gas bubbles. Eventually, grain boundary migration stops.

Although the shape of a grain has been approximated by a tetrakaidecahedron with its 14 flat faces, examination of the microstructures in Fig. 8.1 reveals that the boundaries are slightly curved. This curvature provides the mechanism for movement of the grain boundary.

A small section of a curved grain boundary is shown in Fig. 8.10. The side labeled "concave grain" represents a large grain. The "convex grain" is the adjacent small grain that shrinks as the large grain grows and the grain boundary moves to the left.

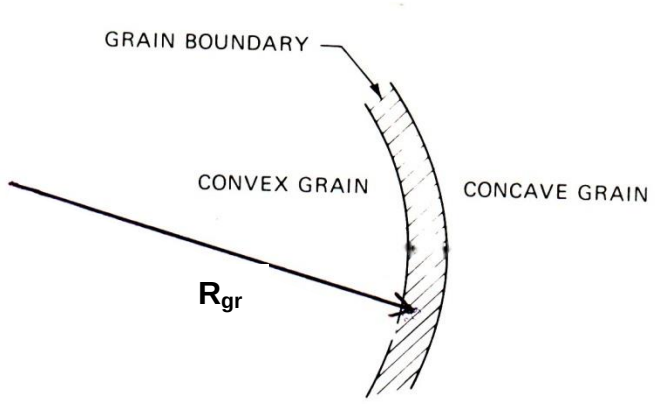

Fig. 8.10 Geometry of a curved portion of a grain boundary

The excess energy of a grain boundary with respect to the perfect lattice of the grain interior is expressed in a manner analogous to surface tension of a solid or liquid.. The property γ_{gb} can represent either the excess energy per unit grain boundary area (units of J/m^2) or as a force acting tangentially to the boundary (units of N/m). Resolving this force in the direction of the radius of curvature produces a negative pressure $2\ \gamma_{gb}/\rho$ on the grain boundary, where ρ is the magnitude of the radius of curvature.

8.2.1 Hillert's model

In general, velocity can be expressed as the product of the mobility M of an object times the force acting on the object. The grain boundary in Fig. 8.10 moves to the left with the velocity:

$$\mathbf{v_{gb} = M\frac{\gamma_{gb}}{\rho}} \tag{8.4}$$

The *ad hoc* relationship adopted by Hillert for the radius of curvature is:

$$\mathbf{\frac{1}{\rho} = \frac{1}{R_{crit}} - \frac{1}{R_{gr}}} \tag{8.5}$$

where R_{gr} is the radius of the grain and R_{crit} is a critical radius below which the grain shrinks and above which the grain grows. Combining these two equations gives the basic equation of the Hillert analysis:

$$v_{gb} = \frac{dR_{gr}}{dt} = Mg_{gb}\left(\frac{1}{R_{crit}} - \frac{1}{R_{gr}}\right) = \mathbf{\frac{M\gamma_{gb}}{\rho}} \tag{8.4a}$$

Equation (8.4a) can be transformed into the following form:

$$\frac{du^2}{d\tau} = \varepsilon(u-1) - u^2 \tag{8.6}$$

where:

$$u = R_{gr}/R_{crit} \qquad \tau = \ln R_{crit}^2 \qquad e = Mg_{gb}/(dR_{crit}^2/dt) \tag{8.7}$$

τ is a surrogate time because, as shown below, R_{crit} increases monotonically with time.

Equation (8.6) is plotted in Fig. 8.11 with ε as a parameter. If $\varepsilon < 4$, $du^2/d\tau$ is negative for all grain sizes u, so that all grains shrink. This is physically impossible because the volume of the solid does not change during grain growth. Similarly, for $\varepsilon > 4$, grains with $u < u_A$ shrink and disappear. Grains with $u > u_B$ shrink until they reach u_B and grains in the range $u_A < u < u_B$ grow until reaching u_B. This means that u remains constant at u_B. Since u is the grain size relative to the critical grain size, and since the latter increases with time, so would the actual grain size. This indefinite increase in R with time is physically impossible. Hillert's conclusion is that the only physically acceptable value of ε is 4, for which Eq (8.6) reduces to:

$$\frac{du}{d\tau} = -\frac{(2-u)^2}{2u} \tag{8.8}$$

The function on the right-hand side has its maximum at u = 2, at which point $du/d\tau = 0$. At all other values of u, $du/d\tau$ is negative. Grains of relative size u > 2 cannot exist because they shrink

until u = 2. The conclusion is that there are no grains in the distribution with radii greater than twice the critical radius, or the maximum value of u in the distribution is 2.

The time rate of change of the critical radius is obtained from the last equation of Eq (8.7) with ε = 4:

$$\frac{dR_{crit}^2}{dt} = Mg_{gb} \tag{8.9}$$

so that R_{crit} increases as $t^{1/2}$.

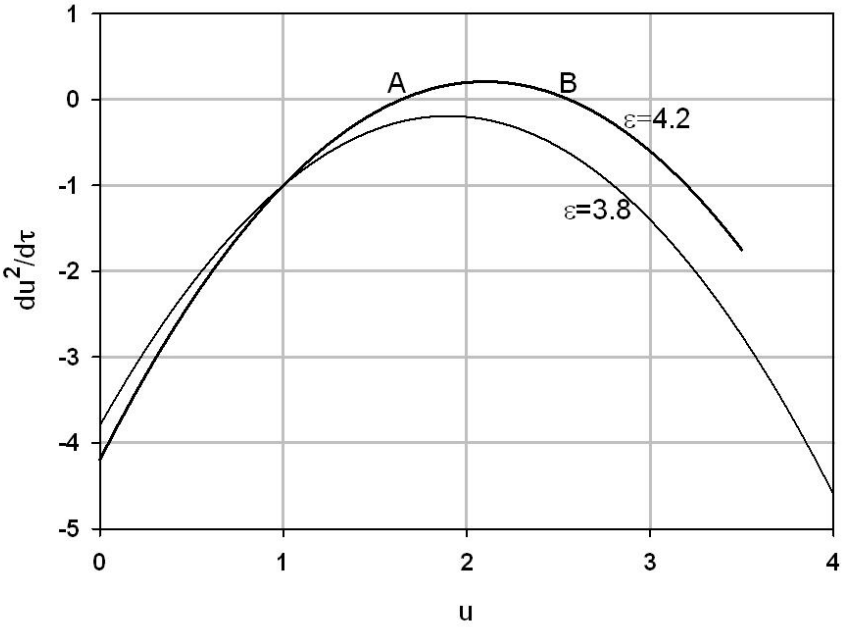

Fig. 8.11 Plots of Eq (8.6)

8.2.2 Grain-size distribution.

Determination of the distribution of grain sizes, such as in Fig. 8.1, begins with the *continuity equation in grain-size space*. This equation is similar in meaning to: i) the slowing-down equation for neutrons in energy space; ii) the coalescence of bubbles in a solid in bubble-size space; and iii) the mass continuity equation for fluids in real space. Figure 8.12 shows how the variables the grain-size continuity equation relate to those of the common the fluid mass continuity equation. The function φ(u,τ) denotes the number of grains in the size range u to u+du at "time" τ; it is the analog of the fluid density in the mass continuity equation. The dimensionless grain size u corresponds to spatial dimension x in the fluid flow situation. The product φdu/dτ is similar in form to the product ρv, where v is the fluid velocity. The fluid mechanics analog variables are shown in **bold** parentheses in Fig. 8.12 next to the grain-size variables.

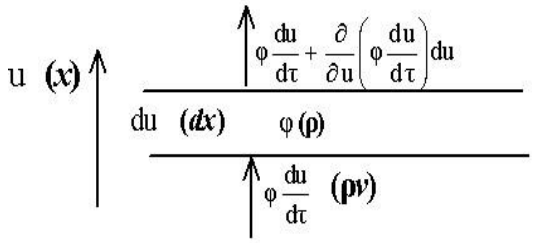

Fig. 8.12 Diagram for deriving the continuity equation in grain-size space. The quantities in bold parentheses next to the parameters are the equivalents for mass continuity in a fluid

The grain-size continuity equation equates the time rate of change of the number of grains in a differential size range du to the net input of grains of size u into this differential element by growth. This is expressed by the equation:

$$\frac{\partial \varphi}{\partial \tau} + \frac{\partial}{\partial u}\left(\varphi \frac{du}{d\tau}\right) = 0 \tag{8.10}$$

The boundary conditions for the continuity equation are: $\varphi = 0$ at $u = 0$ and $u = 2$. Instead of an initial condition, the solution incorporates the requirement that the physical size of the system of grains

$$\frac{4}{3}\pi \int_0^2 R_{gr}^3 \varphi(u,\tau)du$$

be independent of time (or τ). With $du/d\tau$ the function of u given by Eq (8.6), Hillert obtains a solution for φ by rather unorthodox means. To eliminate a constant of integration, the expression for φ is divided by the total number of grains, given by:

$$N(\tau) = \int_0^2 \varphi(u,\tau)du$$

which yields the desired probability distribution of grain sizes, $P = \varphi/N$, or
P(u)du = probability that the size of a grain lies between u and u+du:

$$P(u) = \frac{24u\,e^3}{(2-u)^5}\exp\left(-\frac{6}{2-u}\right) \tag{8.11}$$

where e is the base of the Naperian logarithm. Equation (8.11) is plotted in Fig. 8.13.

There is no explicit dependence of P on τ, which means that the distribution is self-preserving. If P were plotted as a function of grain radius R_{gr}, with time the distribution would shift to larger grain sizes but preserve its shape. The shift in time is a consequence of the definition of u given by Eq (8.7), $R_{gr} = uR_{crit}$, with time dependence of R_{crit} given by Eq (8.9).

The average grain radius is obtained from:

$$\bar{u} = \frac{\bar{R}_{gr}}{R_{crit}} = \int_0^2 u\,\varphi(u,\tau)du = \frac{8}{9} \qquad (8.12)$$

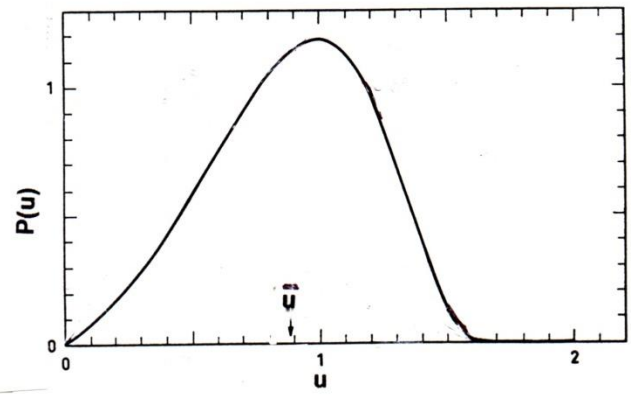

Fig. 8.13 Hillert's grain-size distribution probability function

Other models of grain-size distribution have been proposed with even better fits to the data than Hillert's theory.

8.2.3 Average grain size

If the mobility M of the grain boundary and the energy per unit area of the grain boundary γ_{gb} are known, integration of Eq (8.9) provides the increase of the critical grain radius R_{crit} with time. Multiplication of R_{crit} by 8/9 according to Eq (8.12) yields the mean grain radius. However, $\bar{R}$ is the mean radius in 3 dimensions, and is experimentally inaccessible. What are available are photomicrographs such as those on the right of Fig. 8.1. These are images of a section cut through the polycrystalline solid, and as such represent the grain structure in 2 dimensions. What is termed "grain size" in all applications is the average diameter of the grains seen in the photomicrographs, designated as d. Hillert gives the relationship of the 3D and 2D grain sizes as:

$$\bar{R}_{gr} = 0.89(d/2) \qquad (8.13)$$

Experimentally, the grain diameter is identified with the "mean intercept length", which is obtained as follows. On a photomicrograph showing the grain structure, a straight line is drawn (Fig. 8.14). The line need not pass through the center of the photomicrograph; any line will suffice. The length of the line on the photomicrograph (L) is measured and then divided by the the number of intersections of the line with grain boundaries (n). For example, using the scale on the lower left in Fig. 8.14, the length of the line is 535 μm. There are 6 intersections of the line with grain boundaries, yielding a grain diameter of 90 μm. The general formula for this method is:

$$d\ (\mu m) = L\ (\mu m\ )/n$$

Higher accuracy is obtained by drawing many lines on the photomicrograph and for each, determining d from the above formula. The average value is the best estimate of the 2D grain diameter.

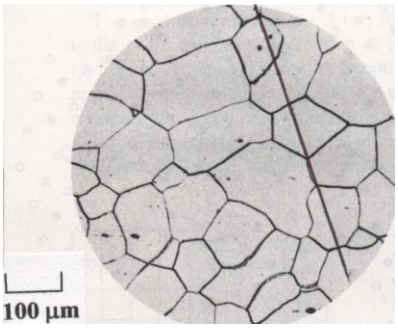

length = L

Fig. 8.14 Photomicrograph with arbitrary line drawn on it.

8.2.4 Grain Growth

Eliminating R_{crit} from Eq (8.9) using Eq (8.12), replacing $\overline{R}_{gr}$ by d using Eq (8.13) and integrating yields:

$$d^2 - d_o^2 = \left(\frac{4}{0.89^2} \frac{32}{81} M \gamma_{gb} \right) t = k_{gg}\, t \qquad (8.14)$$

which is the classical parabolic grain-growth law. d_o is the initial mean grain diameter. The quantity in parentheses is a function of temperature only, and is called the *grain-growth constant* (k_{gg}, $\mu m^2/s$). The particular form of k_{gg} in Eq (8.14) applies only to Hillert's model.

Preferred orientation and the collection of impurities at grain boundaries usually force deviations from the parabolic form of Eq (8.14).

8.3 Grain Boundary Mobility

The grain boundary mobility M in Eq (8.14) is intimately related to the curvature of the grain boundary. As suggested by Fig. 8.10, a lattice atom (or, in the case of ceramics, an ion) on the convex side of the grain boundary has slightly fewer neighbors to bind to than one on the concave side. Consequently, the potential energy of atoms on the convex side of the boundary is slightly greater than those on the concave side. The variation of the potential energy of an atom/ion as it moves between the two sides of the grain boundary is shown in Fig. 8.15.

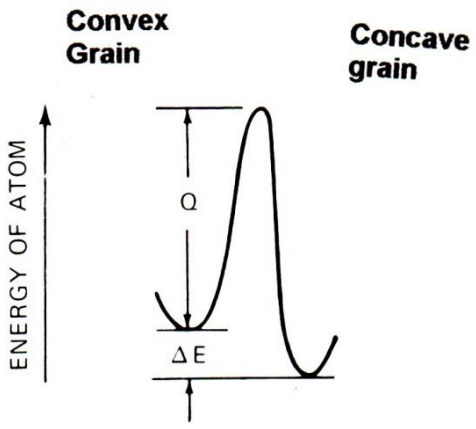

The extra potential energy of atoms/ions at the boundary in the convex side of the grain is denoted by ΔE, which is much smaller than the activation energy Q for atom motion across the barrier. The frequency with which an atom jumps over the barrier in a particular direction is the

vibration frequency in the equilibrium site, ν, times a Boltzmann factor (Eq (5.31)). Because of the difference in the barrier heights, the barrier-crossing frequency is slightly greater for convex-to-concave jumps than for those in the reverse direction. The net flux of atoms from the convex side to the concave side, J_{net}, equals the difference in the jump frequencies multiplied by the

Fig. 8.15 Potential energy of an atom on two sides of a curved grain boundary

number of atoms per unit area in the grains abutting the boundary, which approximately is $1/a_o^2$, a_o being the lattice constant. Finally, the velocity of the grain boundary, which is in the opposite direction to the atom flux, is the product of the flux and the atomic volume Ω, the latter approximated by a_o^3. The result is:

$$v_{gb} = a_o^3 J_{net} = a_o^3 \frac{1}{a_o^2}\left[\nu \exp\left(-\frac{Q}{k_B T}\right) - \nu \exp\left(-\frac{Q+\Delta E}{k_B T}\right)\right] \cong \nu a_o \frac{\Delta E}{k_B T}\exp\left(-\frac{Q}{k_B T}\right) \tag{8.15}$$

The last form arises from approximating the second exponential term by a Taylor series expansion, owing to $\Delta E << k_B T$.

In order to relate ΔE to macroscopic quantities, we calculate the work to move atoms from the concave to the side convex of the boundary. This causes the boundary in Fig. 8.10 to move to the right, say by a distance dr. The macroscopic force (per unit area) resisting this movement is γ_{gb}/ρ (ρ from Eq (8.5), so that the work per unit area is (γ_{gb}/ρ)dr. The volume displaced, dr (per unit area) involves dr/Ω atoms. Dividing the former by the latter gives the work performed per atom moved, which is identified with net change in potential energy in Fig. 8.15. Thus:

$$\Delta E = \gamma_{gb}\Omega/\rho \tag{8.16}$$

where ρ is the radius of curvature of the grain boundary. Substituting Eq (8.16) into Eq (8.15), equating the result to the right hand side of Eq (8.4a) and solving for the mobility gives:

$$M = \frac{n a_o W}{k_B T}\exp\left(-\frac{Q}{k_B T}\right) \tag{8.17}$$

Example #2 - Grain-boundary velocity

What is the velocity of a grain boundary with a 15μm radius-of-curvature in UO_2 at 2000 K?
$\nu = 10^{13}$ s^{-1}; $a_o = 5.47\text{x}10^{-10}$ m; $\Omega = 4.0\text{x}10^{-29}$ m^3; $\gamma_{gb} = 0.3$ N/m; Q = 364 kJ/mole (Ref. 5), $k_B = 1.38\text{x}10^{-23}$ J/K

Substituting the above parameters into Eq (8.17) gives M = $2.4\text{x}10^{-15}$ (m/s)/(N/m^2).
From Eq (8.3):

$$v_{gb} = 2.4 \times 10^{-15}\frac{0.3}{15 \times 10^{-6}} = 4.8x10^{-11} \text{ m/s} \quad (4 \text{ mm/d})$$

What is the grain-growth constant when the mean grain size is 20 μm?
The grain growth constant is equal to the quantity in parentheses in Eq (8.14):

$$k_{gg} = \tfrac{4}{0.89^2}\tfrac{32}{81}(2.4 \times 10^{-15}) \times 0.3 = 1.4\text{x}10^{-15} \text{ m}^2/\text{s}$$

Taking the derivative of Eq (8.14):

$$\frac{d(d)}{dt} = \frac{k_{gg}}{2d} = \frac{1.4 \times 10^{-15}}{2 \times 20 \times 10^{-6}} = 3.6 \times 10^{-11} \text{ m/s} = 3 \text{ μm/d}$$

Second phases in a solid often serve to retard the motion of grain boundaries. Pores in ceramics are a common impediment to grain growth. When a moving grain boundary encounters a pore, the system energy is decreased because the empty space of the pore reduces the area of the grain boundary. The grain boundary either drags the pore along with it at a reduced velocity or pulls away from the pore and moves on. This aspect of grain growth is discussed in detail elsewhere (Ref. 4, p. 280). With second-phase retardation, the grain growth rate loses its parabolic character, and Eq (8.14) is replaced by the following more general form:

$$d^n - d_o^n = k_{gg} t \tag{8.18}$$

where n is 3 or 4, or sometimes a noninteger. The constants n and the temperature-dependent k_{gg} are usually determined experimentally.

8.4 Grain Boundary Diffusion

Grain boundaries are fast-diffusion paths that are characterized by much higher diffusion coefficients than those in the lattice. The grain boundary atomic structure is more open than the atom packing in the lattice. Impurity atoms or host atoms in a grain boundary experience a lower energy barrier for migration than they do than in the crystal lattice. This means that grain-boundary, or *intergranular*, diffusion increasingly dominates volume, or *intragranular* diffusion as the temperature is reduced. This characteristic temperature effect holds for all polycrystals.

The diffusing species surrounds grains deep inside the specimen and provides the driving force for the slower lattice diffusion into the grain interior. Figure 8.16 shows the results of PuO_2 penetration into polycrystalline UO_2. The scans of Pu alpha radioactivity on the left demonstrate extensive transport of Pu into the UO_2 via the grain boundary. The electron-microprobe pictures on the right show the very shallow penetration of Pu into the interior of the UO_2 grain.

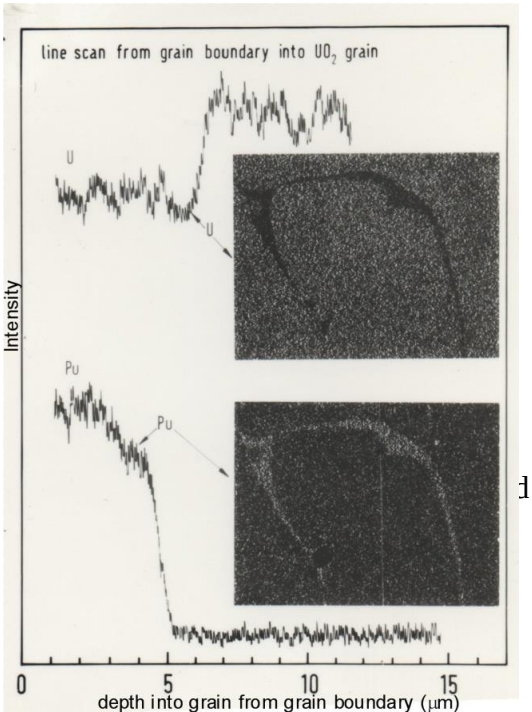

8.4.1 Measurement of the Grain-Boundary Diffusivity

The classical method for determining D_{gb} in polycrystals is the instantaneous source method. This technique has been described in Sect 5.3.2 for volume diffusion as the sole transport mode (i.e., for single crystals).

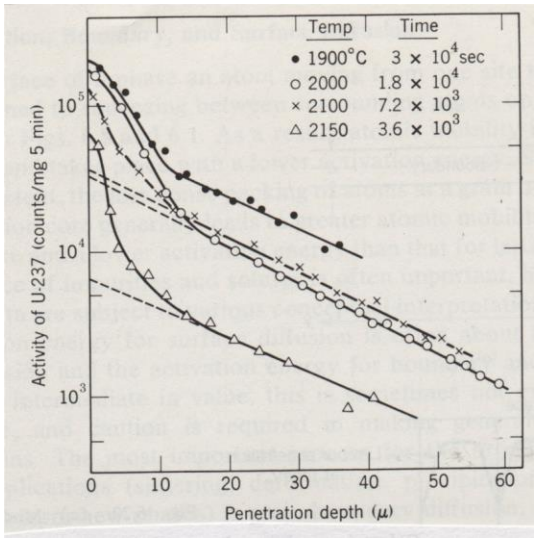

Fig. 8.17 U-237 profiles from an instantaneous surface source on UO_2

Figure 8.17 shows the penetration of radioactive ^{237}U from a thin surface layer into a bulk UO_2 specimen. The quantity measured is the cation (U^{4+}) self-diffusion coefficient. The initial portion of the curves arises from volume diffusion directly into the grains at the surface, and is given by Eq (5.12). The long tails of the penetration profiles are due to diffusion along the grain boundaries. Clearly the depth of penetration indicates that atom mobility in the grain boundaries is greater than in the lattice.

The theoretical analysis of this problem is complicated by the need to the couple the diffusion equation in the grain boundaries to that within the grains. This coupling occurs in two places:
i) the grain-boundary diffusion equation contains a sink term due to volume diffusion into the grains;
ii) the boundary condition for the lattice-diffusion equation reflects the equality of the concentration in the grain boundary and that in the lattice at the grain periphery.

This mathematical problem has been attacked by researchers for fifty years. The most commonly-used result is that of Levine and MacCallum (Ref. 6) who showed that the logarithm of the tracer concentration varies as the 6/5 power of the depth x[2] Thus, the grain-boundary contribution to the penetration profile is clearly separable from the volume diffusion portion, for which the logarithm of the concentration of the diffusing species varies as the square of the depth x (Eq. (5.12)). The grain boundary diffusion coefficient in UO_2 can be extracted from the deep-

[2] The points in the tails of the curves in Fig. 8.17 plot linearly with x or $x^{6/5}$

penetration portion of the curves in Fig. 8.17 using the equation: $dD_{gb} = 0.66\sqrt{Dt}\left(\frac{d\ln c_{gb}}{dx^{6/5}}\right)^{5/3}$ (8.19)

In this formula, δ is the thickness of the grain boundary , D is the volume diffusion coefficient, and x is the penetration depth. Note that only the product δD_{gb} can be determined from the experiment. Other techniques are required to separate these two parameters (see Ref.1)

Figure 8.18 shows Arrhenius plots of the two diffusivities in UO_2. The activation energy (the slope of a line) is greater for volume diffusion than it is for grain-boundary diffusion. Also notable is the very large difference between the two diffusivities at low temperatures. It is clear that at low temperatures, grain boundary diffusion is the primary mode of atom movement.

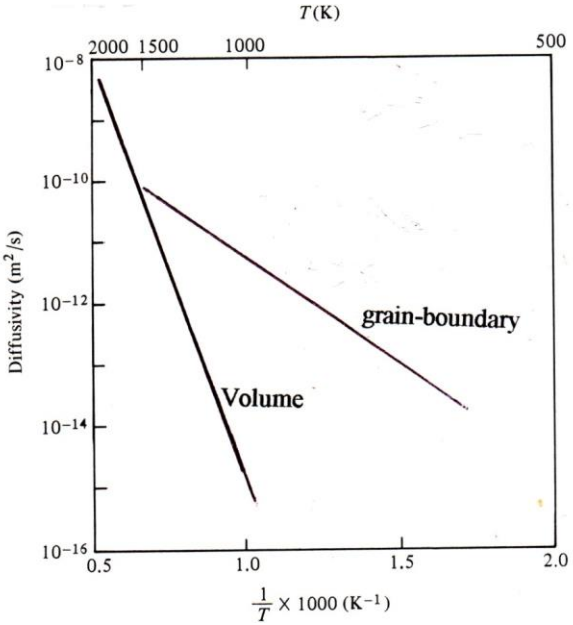

Fig. 8.18 Arrhenius plots of volume and grain-boundary self-diffusion coefficients in UO_2

8.4.2 Effect of Grain Boundary Diffusion on Fission Product Release

The release of volatile fission products (iodine, tellurium) from ceramic nuclear fuel involves the two diffusion processes shown in Fig. 8.19. This sketch depicts the grains in UO_2 and the path followed by fission products generated in the grains. Volatile fission products escape easily from the surface, so the rate-limiting steps are the series processes of volume diffusion followed by grain-boundary diffusion to the free surface.

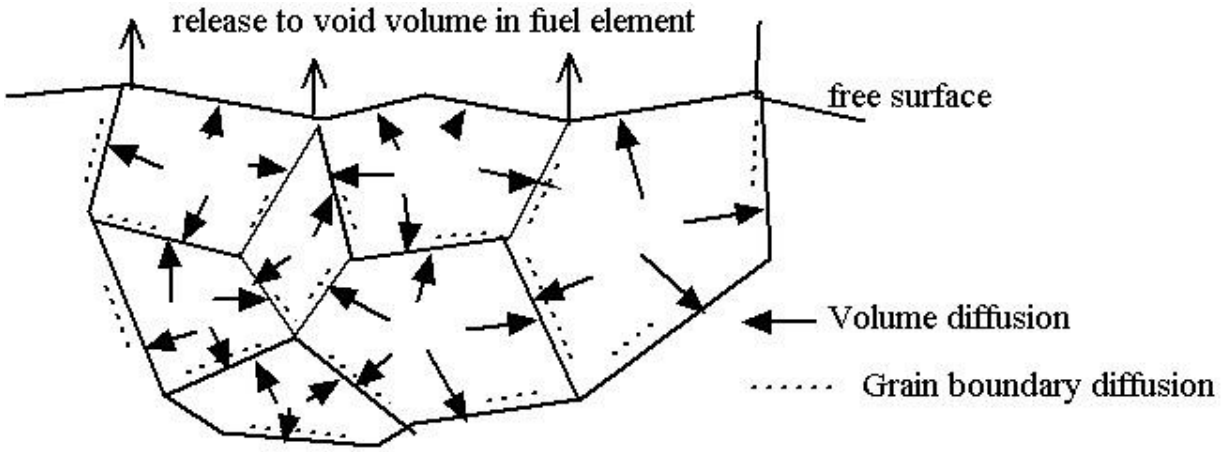

Fig. 8.19 Schematic of path of fission product release by combined lattice and grain-boundary diffusion to a free surface

Mathematical simulation starts with release by volume diffusion from the grains, which are modeled as spheres of radius $\mathbf{R_{gr}}$. The volatile fission products have no thermodynamic solubility in UO_2, which means that once they reach a grain boundary, they are permanently retained there. I Insolubility is equivalent to requiring that the concentration of the intragranular fission product is zero at the grain surface, despite the nonzero concentration in the grain boundary. This condition decouples the volume diffusion in the grains from the subsequent grain-boundary diffusion step. The analysis of the former in Appendix C of Chap. 5 shows that the average fission-product concentration in the grain decreases with time according to Eq (5C.11):

$$\frac{\bar{c}}{c_o} = 1 - \frac{6}{\sqrt{\pi}}\sqrt{\tau} + 3\tau \qquad (8.20)$$

where $\tau = Dt/R_{gr}^2$ is the dimensionless time and c_o is the initial concentration in the grains.

The specimen geometry for the grain-boundary diffusion step is taken to be a thin disk of polycrystalline solid (below):

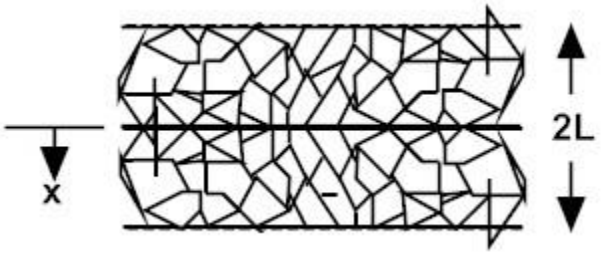

Disk thickness = 2L
The heavy line denotes the midplane

.

This is representative of the post-irradiation annealing experiment described in Sect. 5.3. The distance from the midplane of the disk is denoted by x, so the grain boundary diffusion process takes place in $0 \le x \le L$.

The flux of fission product along grain boundaries per unit area in the x direction is:

$$J_{gb} = -\sigma D_{gb} \frac{\partial \varphi}{\partial x} \tag{8.21}$$

D_{gb}, the grain boundary diffusion coefficient, has the same units as its three-dimensional counterpart, namely length squared per unit time.
φ = diffusing species per unit area of grain boundary
σ = total grain-boundary area in a unit volume of solid (see Sect. 8.1).

Representing the grains as spheres of radius R_{gr} , the grain boundary area per unit volume is:

$$\sigma = \frac{3}{2R_{gr}} \tag{8.22}$$

The total quantity of diffusing solute per unit volume contained in the grain boundaries is:

$$c_{gb} = \sigma\varphi. \tag{8.23}$$

The species conservation equation is analogous to that for ordinary volume diffusion shown in Fig. 5.1 with J replaced by J_{gb} and c (volume concentration in grains) replaced by c_{gb}. In Eq (5.1), the source term Q becomes $-d\bar{c}/dt$, because all fission product released from the grains is received by the grain boundaries. Using Eq (8.21) in Eq (5.1) results in:

$$\frac{\partial c_{gb}}{\partial t} = \frac{\pi}{4} D_{gb} \frac{\partial^2 c_{gb}}{\partial x^2} - \frac{d\bar{c}}{dt} \tag{8.24}$$

In order to facilitate solution of this equation, distance is made dimensionless using:

$$X = x/L$$

The second term on the right hand side of Eq (8.23) is expressed in terms of $\tau = Dt/R_{gr}^2$ from Eq (8.20). With these substitutions, the grain boundary diffusion equation becomes:

$$\frac{1}{\kappa}\frac{\partial \Phi}{\partial \tau} = \frac{\partial^2 \Phi}{\partial X^2} + \frac{1}{\sqrt{\pi\tau}} - 1 \tag{8.25}$$

where the dimensionless grain-boundary concentration is:

$$\Phi = \frac{\pi}{12}\frac{D_{gb}}{D}\frac{R_{gr}^2}{L^2}\frac{c_{gb}}{c_o} \tag{8.26}$$

where κ is a parameter reflecting the relative importance of grain boundary diffusion to volume diffusion:

$$\kappa = \frac{\pi}{4}\frac{D_{gb}}{D}\frac{R_{gr}^2}{L^2} \tag{8.27}$$

The initial condition assumes that all fission products are in the grains and none in the grain boundaries:

$$\Phi = 0 \quad \text{at} \quad \tau = 0 \tag{8.28}$$

The conditions at the midplane and at the surface are:

$$\partial\Phi/\partial X = 0 \quad \text{at } X = 0 \qquad \text{and} \qquad \Phi = 0 \quad \text{at } X = 1 \tag{8.29}$$

The first of these conditions results from the symmetry condition at the midplane and the second arises from immediate release of fission product to the gas phase upon reaching the specimen surface.

Equation (8.25) subject to Eqs (8.28) and (8.29) can be solved numerically for $\Phi(X,\tau)$ for κ values ranging from 0 (no grain-boundary diffusion) to ∞ (very rapid grain-boundary diffusion). The total fission product concentration (intragranular plus intergranular) is:

$$\bar{c}_{tot} = \bar{c} + \bar{c}_{gb}$$

The desired result is the fraction release: is:

$$f = 1 - \frac{\bar{c}_{tot}}{c_o} = 1 - \frac{\bar{c}}{c_o} - \frac{3}{\kappa}\int_0^1 \Phi(X,\tau)\,dX = \frac{6}{\sqrt{\pi}}\sqrt{\tau} - 3\tau - \frac{3}{\kappa}\int_0^1 \Phi(X,\tau)\,dX \tag{8.30}$$

The first two terms represent the fraction of fission product released from the grains, but not necessarily from the specimen. The last term is the portion of the fission products released from the grains that is retained in the grain boundaries, and therefore does not contribute to the release fraction.

Figure 8.20 shows the time dependence of the fraction release computed from Eq (8.30) over the entire range of κ . For $\kappa = \infty$, the grain-boundary diffusion coefficient is so large that that diffusion in the grains completely controls the release rate. In the opposite limit, as $\kappa \rightarrow 0$, release from the grains is effectively instantaneous and all fission product supplied to the grain boundaries escapes by slow intergranular diffusion.

Example # 3 – Fractional release of a fission product:

i) polycrystalline UO_2, the volume diffusivity is 10^{-13} cm^2/s and the ratio $D_{gb}/D = 10^5$. With grains 10 μm in diameter and a disk 1 mm thick, what is the ratio of the fractional release in 100 hours from the polycrystalline specimen to that from a single crystal of UO_2 of the same thickness annealed for the same period of time?

from Eq (8.27):
$$\kappa = \frac{\pi}{4}\left(\frac{5\times10^{-4}}{5\times10^{-2}}\right)^2 10^5 = 7.9$$

the dimensionless time is:
$$\tau = \frac{Dt}{R_{gr}^2} = \frac{10^{-13}\times3.6\times10^5}{(5\times10^{-4})^2} = 0.14$$

Roughly estimating the fraction release from Fig. 8.20 for these values of κ and τ yields $f_{PC} \cong 0.70$.

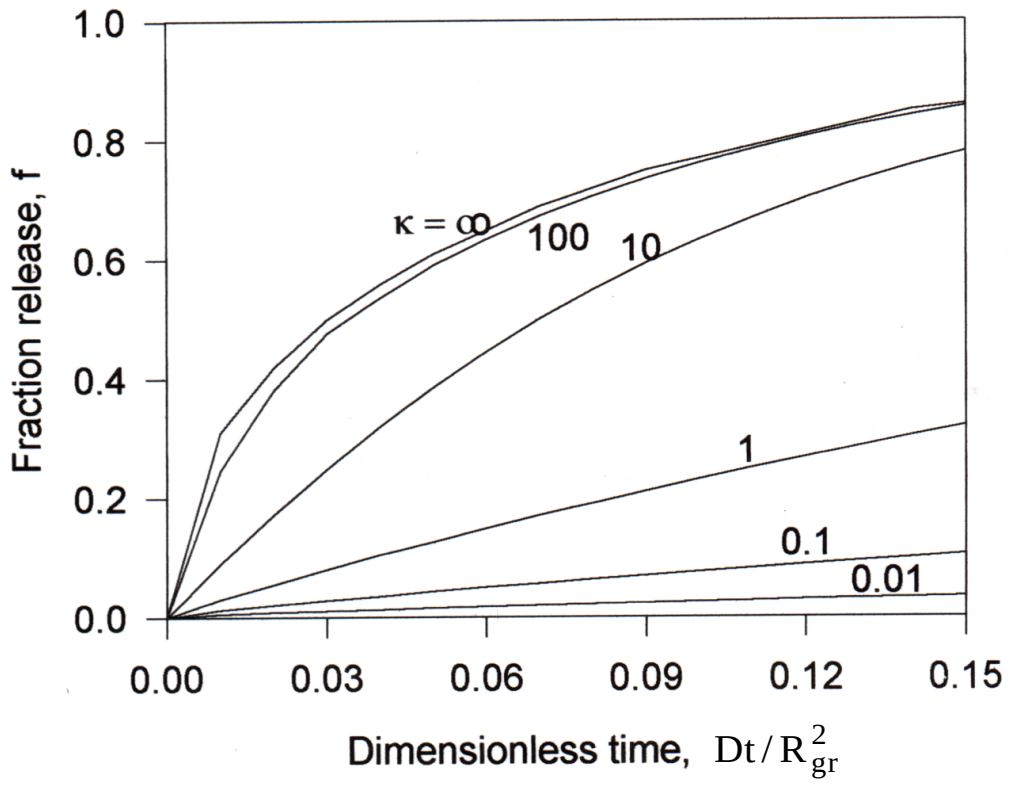

Fig. 8.20 Effect of grain-boundary diffusion on fission product release

ii) single-crystal specimen, the characteristic length is the half-thickness of the disk, L = 0.05 cm. The dimensionless time is

$$\frac{Dt}{L^2} = \frac{10^{-13}\times3.6\times10^5}{(5\times10^{-2})^2} = 1.4\times10^{-5}$$

In principle, the fraction release could be read directly from Fig. 5.3, but in practice, the dimensionless time is too small for this approach.

Alternatively, for such a small time, fission product is removed only from regions of the disk very close to the surface; the disk appears to be infinitely thick for the purpose of the release calculation. With slight modification, the analysis of diffusion in an infinite solid (Eq (5.9a)) can be applied to the present problem

$$c(x,t) = c_o \mathrm{erf}\left(\frac{x}{2\sqrt{Dt}}\right)$$

The fraction release from the single crystal (f_{SC}) is the integral over the half thickness of the disk of the deviation of the concentration c from the initial value c_o divided by the initial quantity:

$$f_{SC} = \frac{\int_0^L (c_o - c)dx}{c_o L} = \frac{\int_0^L (1 - c/c_o)dx}{L} = \frac{1}{L}\int_0^\infty \mathrm{erfc}\left(\frac{x}{2\sqrt{Dt}}\right)dx$$

Replacement of the upper limit of the integral by infinity is permissible because the complementary error function becomes zero long before the midplane at x = L is reached. The fraction release from the single crystal is[3]:

$$f_{SC} = \frac{2}{\sqrt{\pi}}\sqrt{\frac{Dt}{L^2}} = \frac{2}{\sqrt{\pi}}\sqrt{1.4\times10^{-5}} = 4.3\times10^{-3} \qquad (8.31)$$

The ratio $f_{PC}/f_{SC} = 0.70/4.3\text{x}10^{-3} = 160$. For this example, the presence of grain boundaries in the specimen is a very important aid to release of the fission product.

8.5 Sintering

Sintering means removal of porosity in a solid, generally by heating to a high temperature in order to achieve a sufficiently large diffusivity of the point defect responsible for moving atoms from grain boundaries or the grain interior to the pores. Sintering is always accompanied by grain growth, but this combination is not included here.

As shown in Fig. 8.21, there are three stages of sintering. During the initial stage, necks form between adjacent particles and grow until the grains take on the shape of tetrakaidecahedra with open tunnels along the edges (stage 2). These pinch off to form enclosed pores at the corners where four grains meet (stage 3). Grain-boundary movement may leave behind some of these pores, which then become intragranular. Reference [7] covers all three stages, but only stage 3 is analyzed below.

The pores are assumed to be gas-filled spheres of radius R_P located at the corners of the tetrakaidecahedron in Fig. 8.21. There are 6×4 corners of the squares and 8×6 corners of the hexagons, but each corner is shared between 3 faces, so that a single tetrakaidecahedron has 24 corners. In a solid, each corner is shared between 4 tetrakaidecahedra, so that there are

[3] $\int_0^\infty \mathrm{erfc}(u)du = 1/\sqrt{\pi}$

effectively 6 pores per grain. The characteristic dimension of the tetrakaidecahedron is the edge length *l* in terms of which the equivalent sphere diameter is $d_{eq} = 2.785l$ and the volume of the grain is $V_{gr} = 11.31l^3$ (Sect 8.1.3). Eliminating *l*, the grain volume is $V_{gr} = 0.52\, d_{gr}^3$.

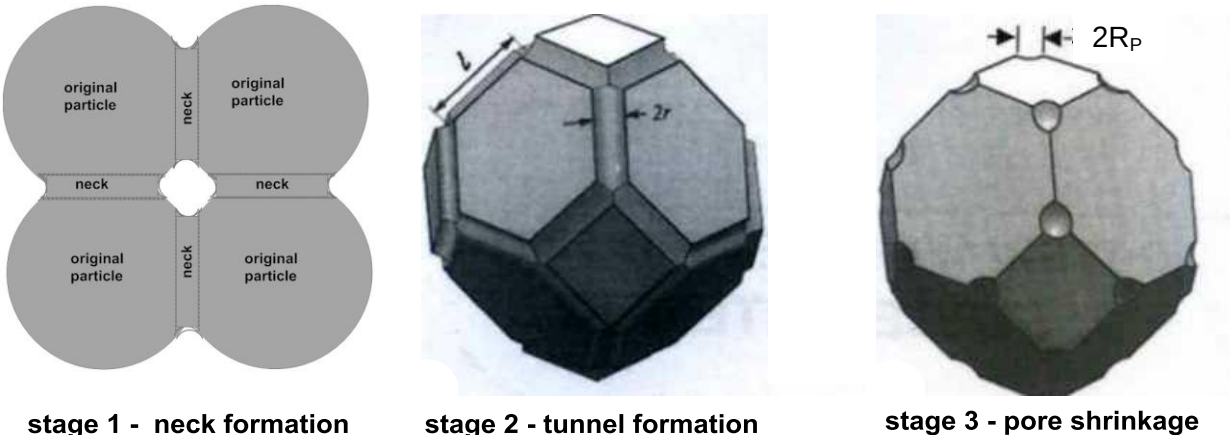

Fig. 8.21 The three stages of sintering (from Ref. 7)

The volume of pores per unit volume (the porosity **P**) is:

$$\mathbf{P} = \frac{\text{pore volume}}{\text{grain volume}} = \frac{6\left(\frac{4}{3}\pi R_P^3\right)}{0.524\, d_{gr}^3} = 48\frac{R_P^3}{d_{eq}^3} \tag{8.32}$$

where R_P is the pore radius.
Grain-boundary transport of vacancies is not considered; all vacancies from a pore diffuse into a bulk solid of effectively infinite extent. Because of the curvature of the pore surfaces, the vacancy concentration C_V^{eq} (in moles per unit volume) is higher at $r = R_P$ than in the bulk solid, $r = \infty$. The pore concentration is small enough that their presence as vacancy sources does not disturb the equilibrium vacancy concentration in the bulk solid.

Because the rate of change of the pore radius is small compared to the time constant with which the concentration profile can adapt, quasi-steady-state diffusion from the pore surface to the surrounding solid is acceptable:

$$\frac{1}{r^2}\frac{d}{dr}\left(r^2\frac{dC_V}{dr}\right) = 0 \tag{8.33}$$

for which the first integral is:

$$\frac{dC_V}{dr} = -\frac{A}{r^2} \tag{8.34}$$

Integration of Eq (8.34) gives:

$$C_V - C_V(\infty) = \frac{A}{r} \tag{8.35}$$

Section 19.2 describes the concentration of vacancies under various conditions; these are employed to establish the boundary conditions for Eq (8.33). The solid is assumed to be subject to a pressure p_o. This is also the gas pressure in the pores when they are first sealed off.

With the boundary condition

$$C_V(\infty) = (C_V^{eq})_o \exp\left(-\frac{p_o\Omega}{k_B T}\right) \text{ at } r = \infty \qquad (8.36a)$$

At the surface of the pore:

$$\mathbf{C_V(R_P) = (C_V^{eq})_o exp\left[\left(\frac{2\gamma}{R_P} - p\right)\frac{\Omega}{k_B T}\right]} \qquad (8.36b)$$

where:

γ = surface tension of solid, N/m or J/m^2
Ω = molecular volume, m^3/molecule
p = pressure inside cavity, N/m^2 (Pa)
$k_B = 1.38\times10^{-23}$ J/K = Boltzmann's constant
T = temperature, K
$\mathbf{(C_V^{eq})_o}$ = equilibrium vacancy concentration at T and 1 atm pressure

Inserting Eqs (8.36a) and (8.36b) into Eq (8.35), and assuming that the argument of the exponential is small enough that $e^x \sim 1 + x$ gives the integration constant A:

$$\mathbf{A = R_P(C_V^{eq})_o\left(\frac{2\gamma}{R_P} - p + p_o\right)\frac{\Omega}{k_B T}} \qquad (8.37)$$

The time-rate of change of the pore volume is:

$$\frac{d}{dt}\left(\frac{4}{3}\pi R_P^3\right) = \Omega(4\pi R_P^2) D_V\left(\frac{dC_V}{dr}\right)_{RP} \quad \text{or} \quad \frac{dR_P}{dt} = -\frac{\Omega D_V (C_V^{eq})_o}{R_P}\left(\frac{2\gamma}{R_P} - p + p_o\right)\frac{\Omega}{k_B T} \qquad (8.38)$$

Assuming the ideal gas law to apply, the pressure in the cavity is:

$$p = p_o(R_{Po}/R_P)^3 \qquad (8.39)$$

where R_{Po} is the pore radius at the start of stage-3 sintering. Substituting Eq (8.39) into Eq (8.38) gives the shrinkage rate as:

$$\frac{dR_P}{dt} = -\frac{\Omega D_V (C_V^{eq})_o}{R_P}\left(\frac{2\gamma}{R_P} - p_o\frac{R_{Po}^3}{R_P^3} + p_o\right)\frac{\Omega}{k_B T} \qquad (8.40)$$

which is to be integrated with the initial condition $R_P = R_{Po}$ at t = 0.

Integration is simplified if this equation is recast in dimensionless terms, with:

$$h = \frac{R_P}{R_{Po}} \qquad t = \frac{t}{t^*} \quad with \quad t^* = \left(\frac{\Omega D_V (C_V^{eq})_o}{R_{Po}^2} \frac{\Omega p_o}{k_B T} \right)^{-1} \quad and \quad a = \frac{2\gamma}{p_o R_{Po}} \tag{8.41}$$

The dimensionless form of Eq (8.39a) is:

$$\frac{d\eta}{d\tau} = -\frac{1}{\eta}\left(\frac{a}{\eta} - \frac{1}{\eta^3} + 1\right) \qquad \eta(0) = 1 \tag{8.40a}$$

The porosity is proportional to R_P^3, or in dimensionless terms,

$$\mathbf{P} = \eta^3 \mathbf{P_o} \tag{8.42}$$

Integrating Eq (8.40a) numerically and substituting $\eta(\tau)$ into Eq (8.42) gives the porosity reduction as a function of dimensionless time.

Example #4 - Final stage sintering

Integrating Eq (8.40a) requires specification of the dimensionless parameter "a" and the initial porosity P_o. Figure 8.22 shows the result of this calculation for a = 2 and a = 10 and $P_o = 0.1$.

The minimum attainable porosity occurs when the gas pressure in the pore becomes high enough to balance the surface tension. This can be obtained by setting the sum of terms in the parentheses of Eq (8.40a) equal to zero and solving for the final pore radius, η_f. Inserting this result in Eq (8.42) yields the final porosity.

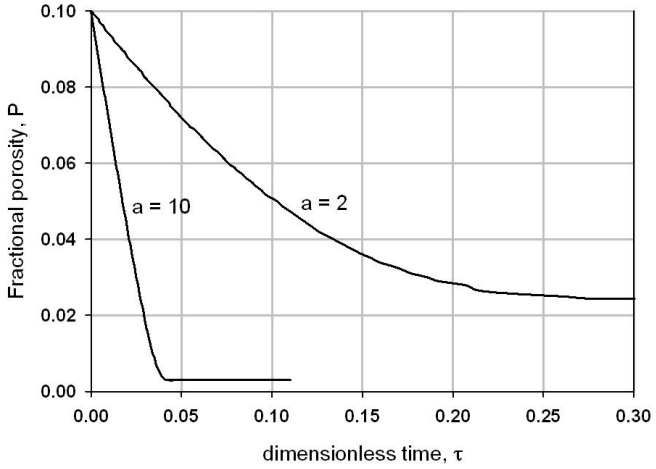

Fig. 8.22 Final stage sintering kinetics

According to Eq(8.41), the principal parameter controlling the dimensionless constant "a" is the initial pore size. R_{Po}. The small initial pore radius gives a = 10, and a five-fold increase in initial pore size produces the a = 2 curve in Fig. 8.22. The former case reaches its final porosity about six times faster than does the large-pore situation. The final porosity in the small-pore calculation is much smaller than that for a = 2 because there is less gas in the small pores than in the large ones.

References

1. I. Kauer, Y. Mishin and W. Gust, *"Fundamentals of Grain and Interphase Boundary Diffusion*", 3rd Ed., Wiley, Chap. 6 (1995)
2. C. R. Barrett, W. D. Nix and A. S. Tetelman, "*The Principles of Engineering Materials",* p. 89, Prentice-Hall (1973)

3. M. Hillert, "*On the Theory of Normal and Abnormal Grain Growth",* Acta Metall. **13** (1965) 227
4. D. R. Olander, "*Fundamental Aspects of Nuclear Reactor Fuel Elements*", National Technical Information Service document No. TID-26711-P1 (1976)
5. J. R. MacEwan and J. Hyashi, Proc. Brit. Ceramic Soc. **7** (1967) 245
6. H. S. Levine and C. J. MacCallum, J. Appl. Phys. **31** (1960) 595
7. Kang, Suk-Joong, *"Sintering, densification, grain growth & microstructure"*, Chaps. 4 & 5, Elsevier (2005)

Problems

8.1. A tetrakaidcahedron (TKDH) provides a good model of grains in a solid. Consider a solid composed solely of TKDHs of edge length L.
a) Prove that the volume of a TKDH is 8 x 21/2L1/3.
b) If the TKDH is sectioned normal to a square face along the face diagonal, an 8-sided figure results. Prove that the area of this section is 7L2.
Hint: The TKDH is an octahedron with its six corners truncated one-third of the distance from each apex. Half of an octahedron is a regular pyramid
8.2. Grain boundaries are internal surfaces of solids. Consider a cubical specimen of solid having 1 cm long sides that is composed of grains shaped like tetrakaidcahedrons (TKDHs) of 100 micron edge length. What is the ratio of the internal surface area to the external surface area of this specimen? Remember that each internal surface is shared between two grains.
8.3 A moving grain boundary experiences a retarding or drag force due to pores and impurities on the grain boundary. This force was neglected in the derivation of Hillert's model, which was based only on the inherent mobility of the pure grain boundary. The drag force is proportional to the grain boundary velocity and can be modeled as:

$$\frac{d(d)}{dt} = \frac{k_{gg}}{2d} - A$$

Where A is a constant representing the retardation effect. (a) What is the maximum grain size achievable (dmax)? (b) What is the integrated grain growth law in terms of dmax?
8.4 Consider the small-angle grain boundary shown in the figure below .
(a) For a simple cubic lattice in which the lattice constant, a, is equal to the Burgers vector b of the edge dislocations forming the grain boundary, what is the distance between dislocations as a function of tilt angle θ***?***

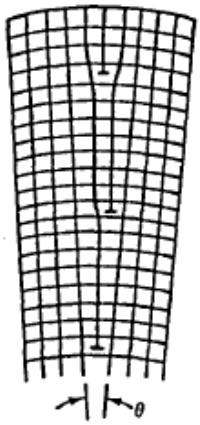

(b) What is the grain boundary tension (energy per unit area) for a tilt angle θ*?* Assume that the extent of the stress field of each dislocation is equal to the spacing between dislocations and that the core radius of the dislocation is 1 Burgers vector.

8.5 For the micrograph below, take a few (3 or 4) measurements of the grain intercepts and use this to calculate the average grain diameter.

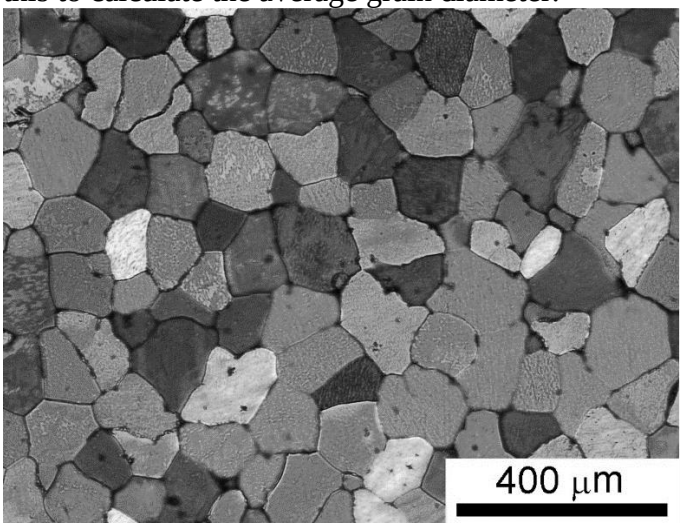

8.6 If sintering is done under compression of the solid, the rate is increased and another parameter is added to the model:

$b = -\sigma P_{Po}/2\gamma$

where σ is the compressive stress (negative stress) and γ is the surface tension of the solid.

(a) What are the units of b?
(b) How are Eqs (8.40) and (8.40a) changed to account for the added stress?

8.7 A lenticular pore is located on the grain boundary of a solid at tensile stress σ. The pore shape is that of two spherical caps of radius R_P joined at the grain boundary.
The pore volume is V. What is the equilibrium shape of the pore (i.e., R_P and θ) .

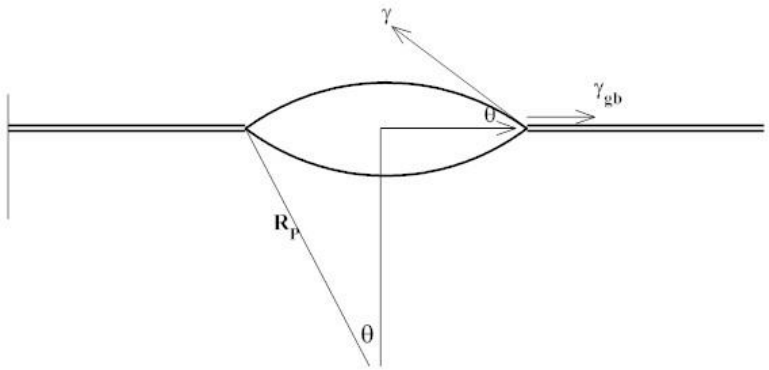

Note: A force balance at the grain-boundary/pore surface junction is needed.
The volume of a spherical cap is $V = 2\pi R_P^3(1-\cos\theta)^2(1-\frac{1}{2}\cos\theta)/3$

8.8 Lenticular fission-gas bubbles form on the faces of grains shaped as tetrakaidcahedra (TKDH). One bubble occupies each of the faces of the TKDH.
At what fractional swelling do the bubbles on adjacent faces touch? (Swelling is defined as the total bubble volume on the 14 faces divided by the volume of the solid)